

# Strategies for Improving Neural Signal Detection Using a Neural–Electronic Interface

Robert B. Szlavik

**Abstract**—There have been various theoretical and experimental studies presented in the literature that focus on interfacing neurons with discrete electronic devices, such as transistors. From both a theoretical and experimental perspective, these studies have emphasized the variability in the characteristics of the detected action potential from the nerve cell. The demonstrated lack of reproducible fidelity of the nerve cell action potential at the device junction would make it impractical to implement these devices in any neural prosthetic application where reliable detection of the action potential was a prerequisite. In this study, the effects of several different physical parameters on the fidelity of the detected action potential at the device junction are investigated and discussed. The impact of variations in the extracellular resistivity, which directly affects the junction seal resistance, is studied along with the impact of variable nerve cell membrane capacitance and variations in the injected charge. These parameters are discussed in the context of their suitability to design manipulation for the purpose of improving the fidelity of the detected neural action potential. In addition to investigating the effects of variations in these parameters, the applicability of the linear equivalent circuit approach to calculating the junction potential is investigated.

**Index Terms**—Nervous system, neural systems, neural electronics, neuron transistor interfacing, neuron transistor.

## I. INTRODUCTION

FROM a historical perspective, techniques for the activation of nerve fibers and for the detection of nervous activity *in vivo* have relied predominantly on nonspecific excitation and detection based on variations in the electric field [1]–[4]. Functional electrical stimulation (FES) is a discipline where specificity associated with nerve fiber excitation and signal detection is highly desirable. One of the predominant issues related to the field-based approach in FES is the inability to specifically control excitation and isolate signal detection at the level of individual nerve fibers [5].

The ability to detect and process individual afferent sensory nerve signals would allow for the possibility of developing more sensitive feedback and control strategies for FES systems. One of the fundamental difficulties associated with detecting signals from individual sensory fibers is related to developing a device that can localize the detection of the signal to the individual fiber and faithfully reproduce this signal while simultaneously rejecting signals associated with the electrical activity of other neurons. Surface electrode approaches to measuring sensory fiber signals suffer from the fact that they are inherently

insensitive to signal localization and instead consist of a summation of the electrical activity in a relatively large area [6]. A better approach to alleviating the localization issue is to use needle electrodes with differential pickup that are inserted near to the sensory fibers of interest. While this approach affords a better spatial localization of the received signal, detection of a signal that represents a cumulative response associated with the electrical activity of several fibers is still possible [6].

Specific nerve cell excitation using a semiconductor based electronic device has been demonstrated by Fromherz and Stett [7]. It has also been demonstrated experimentally by Weis and Fromherz, as well as Vassanelli and Fromherz, that a detectable signal can be conducted from a neuron *in vitro* to a silicon transistor [8], [9]. Direct interface and subsequent signal transduction between individual neurons and single transistors would, if practically achievable in an *in vivo* environment, have the potential of providing a solution to many of the localization issues associated with conventional nonspecific field-based FES sensory nerve signal detection approaches. Based on the nature of the research thus far in neural–electronics, interfacing silicon transistors with unmyelinated axons and small neurons appears to be most feasible at this time. The potential application of this technology to the development of robust neural prosthetics for facilitating the conduction of efferent peripheral nerve signals to muscle groups would seem to be worth investigating. This type of application would require some fundamental research related to implementation of the technology using myelinated axons. Since the transistor forms the common building block for analog integrated circuits, the use of these devices in this application affords the opportunity to incorporate simple signal processing capabilities, such as amplification and filtering of the neural signal, in the front end of a neural interface device. The ability to incorporate integrated analog signal processing capability into the front end of a neural–electronic device would present a definitive advantage since the nature of the signals recorded from neural–electronic devices reported thus far have been of relatively low amplitude [10].

Information content in the nervous system is carried by pulse frequency modulation. It is therefore inherently desirable that any methodology used to detect the neural signal be able to reproduce, with reasonable fidelity, a single pulse as such. Neural–electronics studies presented in the literature, both theoretical and experimental, have reported circumstances in which a dual pulse is produced by the electronic device in response to what is presumed to be a single-action potential in the neuron [10], [11]. A neural–electronic system that was capable of reproducing the neural signal with high fidelity would be better able to preserve the pulse frequency content

Manuscript received November 16, 2001; revised February 5, 2003.

The author is with the Electrical Engineering Department, Louisiana Tech University, Ruston, LA 71272 USA.

Digital Object Identifier 10.1109/TNSRE.2003.810559

of the signal. Moreover, from the perspective of applications related to biosensors for neural toxin detection, as well as the use of these devices for neural activity detection in fundamental electrophysiological research, it is also inherently desirable to employ a detection system in which the characteristics of neural activity are reproduced with reasonably high fidelity. A systematic theoretical analysis of the characteristics of the neural–electronic interface that lead to a high-fidelity reproduction of the neural action potential by the junction potential waveform would yield some insight into approaches for improving the design of the interface region. For the purpose of this study, the characteristic B-type junction described by Weis and Fromherz is considered to be optimal because it most accurately reproduces the characteristics of the action potential [8]. The simulation results of this study suggest that the effect of increasing the seal resistance, which was studied by way of varying the extracellular resistivity parameter, improves the fidelity of the action potential reproduced at the device junction. An increase in the nerve cell membrane capacitance also yields a more faithful reproduction of the nerve cell action potential at the device junction. The simulation results also suggest that decreasing the injected charge yields a more reliable reproduction of the nerve cell action potential at the neural–electronic junction.

Weis and Fromherz [8] also demonstrated that a linear equivalent circuit model representing the nerve cell transistor combination was, under certain circumstances, able to sufficiently reproduce the observed characteristics of the junction potential waveform. They hypothesized that the applicability of the linear approach was due to the quasistatic behavior of the membrane region in close proximity to the transistor gate. The applicability of a linear analysis approach is surprising, given the inherent nonlinear behavior of the neural membrane [12]–[16]. In a subsequent paper, Fromherz proposed various modifications to the conductance properties of the interfaced membrane region that could explain the variations in the characteristics of the junction potential waveforms that have been observed experimentally [10].

Before applying a linear analysis approach, it must be determined whether the linear approximation is generally valid. We investigate this question by specifying an idealized geometry for the neuron and carrying out the neuron–transistor circuit analysis using a nonlinear as well as a linear approach. Based on a previously proposed approach by Fromherz and colleagues [11], the neural membrane is divided into an interfaced and a free region.

It is an inherent assumption of this study that the nonlinear electrical characteristics of the interfaced region of the membrane are not significantly modified by the proximity to the semiconductor oxide layer. There is some preliminary evidence to the contrary that suggests that the transient A-type and constant K-type potassium conductances are modified by the proximity of the cell membrane to the device [17]; however, the mechanism and exact nature of these changes have not, as of yet, been definitively determined.

## II. METHOD

An idealized cylindrical geometry was assumed for the neuron. This geometry was chosen as a simplified approxi-

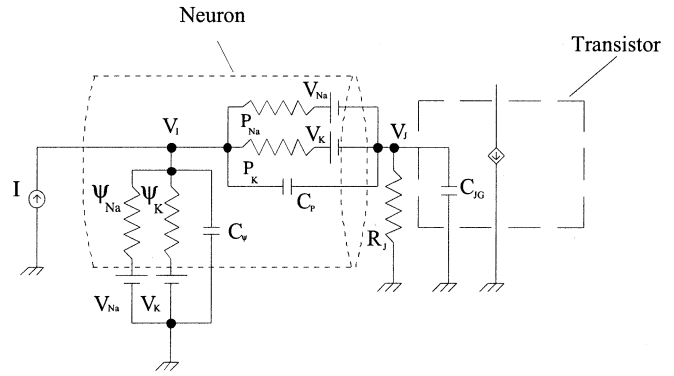


Fig. 1. Nonlinear equivalent circuit model of the neuron–transistor configuration. The equivalent circuit component values are calculated using the physical parameters and formulas shown in Table I.

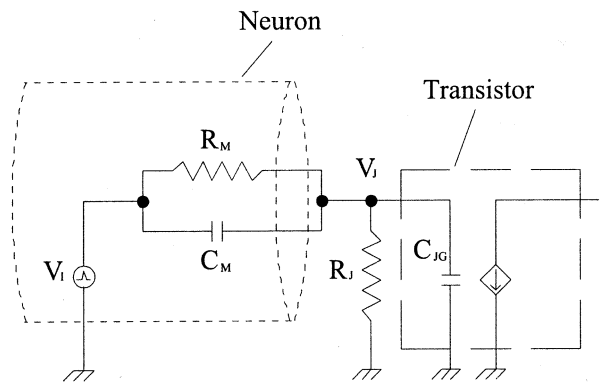


Fig. 2. Linear equivalent circuit model of the neuron–transistor configuration of Fig. 1. The equivalent circuit component values are calculated using the physical parameters and formulas shown in Table I.

mation of the Retzius cell used in neuron–transistor interface experiments presented by Weis and Fromherz [8].

Although the fundamental physical parameters used in determining the equivalent circuit component values shown in Fig. 1 and Fig. 2 are specified in a per-unit-area format, defining the geometric parameters of the neuronal radius  $a_j$  and length  $L$  allow the circuit component values to be specified in absolute units. The physical parameters related to the membrane and the transistor are shown in Table I, along with the definition of the circuit components.

### A. The Nonlinear Equivalent Circuit Model

The nonlinear equivalent circuit that incorporates the nonlinear properties of the membrane is shown in Fig. 1. Based on the Weis–Fromherz hypothesis, this model was developed by dividing the membrane into a region that is interfaced with the electronic device, represented by the  $P$ -labeled circuit components, and a free region of the membrane, represented by the  $\Psi$ -labeled circuit components.

Two separate nonlinear equivalent circuit models are used to represent the surface area of the two distinct regions. The nonlinear circuit with the  $\Psi_{Na}$  and  $\Psi_K$  conductances represents the entire membrane surface excluding the idealized circular region interfaced with the transistor gate. The interfaced region is

TABLE I  
LIST OF THE VARIABLES AND PHYSICAL, AS WELL AS GEOMETRIC, PARAMETERS THAT WERE USED IN THE EQUIVALENT CIRCUIT MODELS AND THE SIMULATION STUDY

$a_j$	Interface region radius and nerve cell radius	10 ( $\mu\text{m}$ )
$d_j$	Nerve cell transistor seal distance	10 (nm)
$L$	Length of the nerve cell	40 ( $\mu\text{m}$ )
$A_\Psi$	Free membrane region area	$\pi a_j^2 + 2\pi a_j L$ ( $\text{cm}^2$ )
$A_P$	Interfaced membrane region area	$\pi a_j^2$ ( $\text{cm}^2$ )
$T$	Temperature	6.3 ( $^\circ\text{C}$ )
$t_i$	Simulation time step	(s)
$k$	Number of time steps	3000
$\rho_J$	Extracellular environment resistivity	( $\Omega\text{cm}$ )
$g_M$	Passive membrane conductance per unit area (linear model)	0.1 ( $\text{mS}/\text{cm}^2$ )
$c_{JG}$	Gate oxide capacitance per unit area	0.3 ( $\mu\text{F}/\text{cm}^2$ )
$c_{Na}^o$	Extracellular sodium ion concentration	0.491 (mol/L)
$c_{Na}^i$	Intracellular sodium ion concentration	0.05 (mol/L)
$c_K^o$	Extracellular potassium ion concentration	0.02011 (mol/L)
$c_K^i$	Intracellular potassium ion concentration	0.400 (mol/L)
$G_{Na}^M$	Maximum sodium conductance per unit area	0.120 ( $\text{S}/\text{cm}^2$ )
$G_K^M$	Maximum potassium conductance per unit area	0.036( $\text{S}/\text{cm}^2$ )
$m$	Hodgkin Huxley first order kinetic variable [16]	
$h$	Hodgkin Huxley first order kinetic variable [16]	
$n$	Hodgkin Huxley first order kinetic variable [16]	
$\Psi_{Na}$	Free membrane region sodium conductance	(S)
$\Psi_K$	Free membrane region potassium conductance	(S)
$P_{Na}$	Interfaced membrane region sodium conductance	(S)
$P_K$	Interfaced membrane region potassium conductance	(S)
$R_J$	Interface junction seal resistance [8]	$\rho_J / (5\pi d_j)$ ( $\Omega$ )
$R_M$	Passive membrane resistance (linear model)	$g_M \pi a_j^2$ ( $\Omega$ )
$c_M$	Membrane capacitance per unit area	( $\text{F}/\text{cm}^2$ )
$C_M$	Membrane capacitance (linear model)	$c_M \pi a_j^2$ (F)
$C_\Psi$	Free membrane region capacitance	(F)
$C_P$	Interfaced membrane region capacitance	(F)
$C_{JG}$	Gate oxide capacitance	$c_{JG} \pi a_j^2$ (F)
$V_{Na}$	Sodium ionic (Nernst) potential	(V)
$V_K$	Potassium ionic (Nernst) potential	(V)
$V_I$	Intracellular potential	(V)
$V_J$	Interface junction potential	(V)
$V_M$	Interface region transmembrane potential	(V)
$V_{NL}$	Calculated junction potential (non-linear model)	(V)
$V_L$	Calculated junction potential (linear model)	(V)
$I$	Injected stimulus current	(A)
$Q_T$	Total injected charge	(C)

modeled by the nonlinear circuit associated with the  $P_{Na}$  and  $P_K$  conductances

$$\begin{aligned}
 \Psi_{Na} &= A_\Psi G_{Na}^M m^3 h \\
 \Psi_K &= A_\Psi G_K^M n^4 \\
 P_{Na} &= A_P G_{Na}^M m^3 h \\
 P_K &= A_P G_K^M n^4.
 \end{aligned} \tag{1}$$

The nonlinear conductances  $\Psi_{Na}$ ,  $\Psi_K$ ,  $P_{Na}$  and  $P_K$  of (1) are defined in terms of the first-order kinetic equation variables  $m$ ,  $h$ , and  $n$ , and their associated rate and time constants, as defined in Weiss [18]. These nonlinear conductances are functions of the transmembrane potential and time.

The coupled ordinary differential equations (2) implemented in the solver routine were written in terms of the intracellular potential  $V_I$  and the transmembrane potential  $V_M$  across the region of the membrane interfaced with the transistor gate (3).

These equations can be derived by applying Kirchhoff's current law to the intracellular and junction nodes

$$\begin{aligned}
 \Psi_{Na}(V_{Na} - V_I) + \Psi_K(V_K - V_I) - C_\Psi \frac{dV_I}{dt} + I + \\
 P_{Na}(V_{Na} - V_M) + P_K(V_K - V_M) - C_P \frac{dV_M}{dt} = 0 \\
 P_{Na}(V_M - V_{Na}) + P_K(V_M - V_K) + C_P \frac{dV_M}{dt} - \\
 \frac{V_I}{R_J} + \frac{V_M}{R_J} - C_{JG} \frac{dV_I}{dt} + C_{JG} \frac{dV_M}{dt} = 0.
 \end{aligned} \tag{2}$$

Since this particular circuit problem can be characterized as an initial value problem, it is necessary to specify the initial values for the intracellular potential variable  $V_I$  and the transmembrane potential  $V_M$ . Prior to excitation, the intracellular potential would assume the resting membrane value. For the specified intracellular and extracellular concentration of ions, the resting membrane potential would assume a value of  $-62.5$  mV.

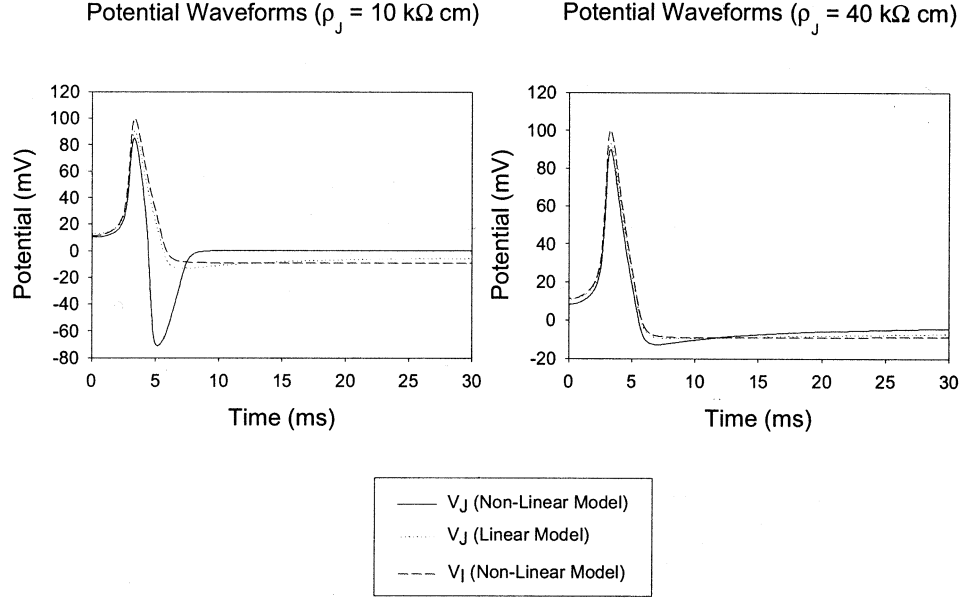


Fig. 3. Potential response plots of the nonlinear and linear equivalent circuit models. The junction potential  $V_J$  for the nonlinear and linear equivalent circuits is shown along with the intracellular potential  $V_I$  calculated from the nonlinear equivalent circuit. Two different graphs are shown for a 10-k $\Omega$ cm and a 40-k $\Omega$ cm extracellular resistivity. The dc component has been removed using a brick-wall filter. A stimulus of 40 nC/cm<sup>2</sup> and a membrane capacitance of 4  $\mu$ F/cm<sup>2</sup> were used.

The junction potential  $V_J$  is initially at equipotential with the extracellular environment, which is at the assigned reference potential. A relationship can be defined between the intracellular junction and transmembrane potentials as

$$V_M = V_I - V_J. \quad (3)$$

A Runge–Kutta ordinary differential equation solver was used to calculate the response of this circuit to a brief 10- $\mu$ s stimulus current pulse.

#### B. The Linear Equivalent Circuit Model

The linear circuit is constructed by replacing the nonlinear membrane components of the surface area associated with the free membrane region with a voltage source that reproduces the  $V_I$  action potential waveform from the nonlinear circuit model of Fig. 1. A representative membrane resistance  $R_M$  and capacitance  $C_M$  are used to replace the nonlinear circuit model associated with the region of the membrane that is interfaced with the transistor gate.

The transfer function of the linear network of Fig. 2 is

$$h(\omega) = \frac{1+a(\omega)}{[1+a(\omega)]^2+b(\omega)^2} - j \frac{b(\omega)}{[1+a(\omega)]^2+b(\omega)^2} \quad (4)$$

where

$$\begin{aligned} a(\omega) &= \frac{R_M R_J + \omega^2 R_M^2 R_J^2 C_{JG} C_M}{R_J^2 + \omega^2 R_J^2 R_M^2 C_M^2} \\ b(\omega) &= \frac{\omega R_J^2 R_M C_{JG} - \omega R_M^2 R_J C_M}{R_J^2 + \omega^2 R_J^2 R_M^2 C_M^2} \end{aligned} \quad (5)$$

and where  $\omega = 2\pi f$ .

### III. RESULTS

#### A. Impact of Extracellular Resistivity

In order to investigate the effects of variations in the junction seal resistance, the extracellular resistivity was varied. The response of the nonlinear equivalent circuit model of Fig. 1 was calculated for an excitatory 10- $\mu$ s stimulus current pulse of 4-mA/cm<sup>2</sup> magnitude and a membrane capacitance of 4  $\mu$ F/cm<sup>2</sup>. For each value of the extracellular resistivity  $\rho_J$ , the intracellular potential  $V_I$ , as well as the junction potential  $V_J = V_I - V_M$ , was calculated. The square root of the sum of the squared differences between the intracellular potential  $V_I$  and the junction potential  $V_J$  was used to quantify the reliability of the reproduction of the nerve cell action potential at the junction as follows, where  $t_i$  is the time step and  $k$  is the number of time steps

$$\delta = \sqrt{\sum_{i=0}^{k-1} [V_I(t_i) - V_J(t_i)]^2}. \quad (6)$$

Fig. 3 is a comparison of the junction potential waveforms calculated for two values of extracellular resistivity. These plots demonstrate that there is an improvement in the reliability of the action potential waveform reproduced at the junction for higher values of the seal resistance  $R_J$  that correspond to higher values of the extracellular resistivity  $\rho_J$ . These graphs also illustrate the consistency of the junction potential waveforms calculated using the nonlinear and linear equivalent circuit models.

Junction potential waveforms calculated using the nonlinear and linear equivalent circuit models exhibit good agreement for larger values of the extracellular resistivity. In the case of the 40-k $\Omega$ cm extracellular resistivity, there is better reproduction of the junction potential waveform by the linear circuit model than

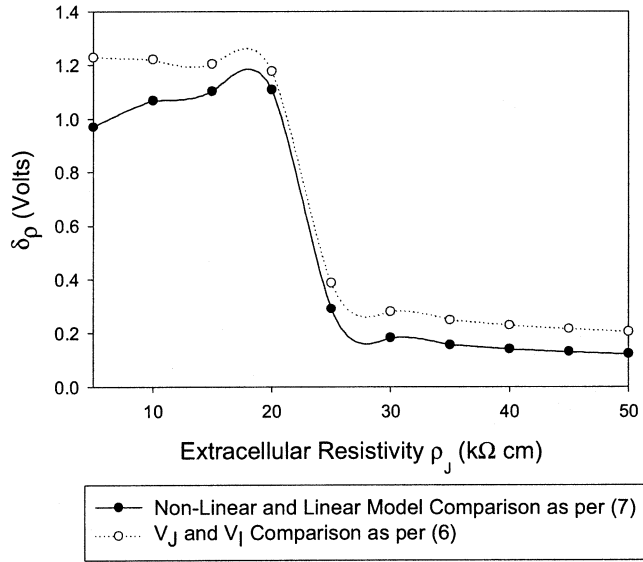


Fig. 4. Norm of the difference between the intracellular potential  $V_I$  and the junction potential  $V_J$  as well as the norm of the difference in junction potentials  $V_J$  between the nonlinear and linear equivalent circuit models as a function of extracellular resistivity. These curves quantify the effectiveness of the linear circuit approximation at reproducing the junction potential  $V_J$  calculated from the nonlinear equivalent circuit model as well as quantifying the reliability with which the intracellular action potential is reproduced at the junction. A stimulus of  $40 \text{ nC/cm}^2$  and a membrane capacitance of  $4 \text{ } \mu\text{F/cm}^2$  were used.

in the  $10\text{-k}\Omega\text{cm}$  case. For the smaller extracellular resistivity values, there is a positive followed by a negative pulse observed at the  $V_J$  node calculated with the nonlinear equivalent circuit model

$$\delta = \sqrt{\sum_{i=0}^{k-1} [V_{NL}(t_i) - V_L(t_i)]^2}. \quad (7)$$

In order to quantify the difference between the junction potential waveforms calculated using the nonlinear and linear equivalent circuit models as a function of the extracellular resistivity, the square root of the sum of the squared differences, as per (7), is plotted in Fig. 4 for the range of values investigated. The junction potentials in (7) calculated using the nonlinear and linear equivalent circuit models are represented by  $V_{NL}$  and  $V_L$ , respectively, where  $t_i$  is the time step and  $k$  is the number of time steps.

Simulation results demonstrate that the difference between the junction potential waveforms calculated using the nonlinear and linear equivalent circuit models, as a function of extracellular resistivity, decreases across the range of values investigated. The results also indicate that a more reliable reproduction of the nerve cell action potential occurs at the junction for higher values of extracellular resistivity.

### B. Impact of Membrane Capacitance

The effect of variations in membrane capacitance on the reliability with which the nerve cell action potential was reproduced at the junction was also studied and quantified, as per (6), for a physiologically relevant range of membrane capacitance values. A significant improvement in the reliability with which the ac-

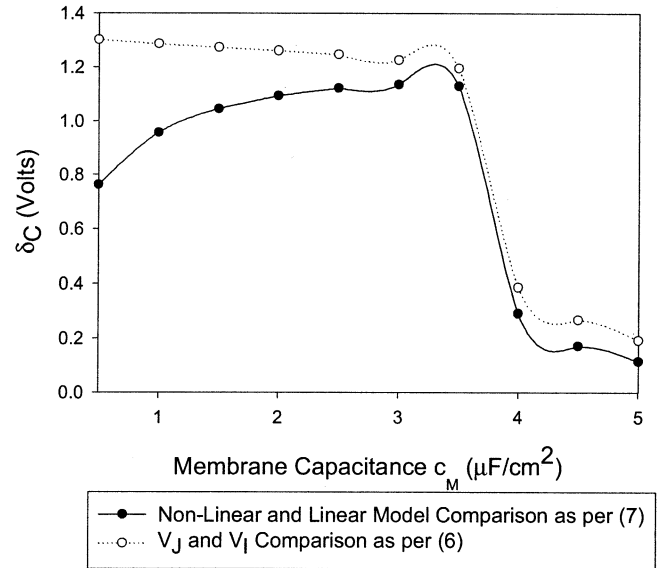


Fig. 5. Norm of the difference between the intracellular potential  $V_I$  and the junction potential  $V_J$ , as well as the norm of the difference in junction potentials  $V_J$  between the nonlinear and linear equivalent circuit models as a function of membrane capacitance. These curves quantify the effectiveness of the linear circuit approximation at reproducing the junction potential  $V_J$  calculated from the nonlinear equivalent circuit model, as well as quantifying the reliability with which the intracellular action potential is reproduced at the junction. A stimulus of  $40 \text{ nC/cm}^2$  and an extracellular resistivity of  $25 \text{ k}\Omega\text{cm}$  were used.

tion potential was reproduced at the junction was observed for larger values of membrane capacitance as per Fig. 5.

The impact of membrane capacitance on the similarity between junction potential waveforms calculated with the linear and nonlinear circuit models was also studied as per (7). An overall improvement in the accuracy with which the linear model reproduces the junction potential waveform calculated using the nonlinear model was observed for larger values of membrane capacitance, as can be seen from Fig. 5.

### C. Impact of Injected Charge

The impact of variations in the amount of injected charge on the reliability with which the nerve cell action potential is reproduced at the junction was studied as per (6). Increasing the amount of injected charge past a threshold value of approximately  $40 \text{ nC/cm}^2$  results in a decrease in fidelity with which the nerve cell action potential waveform is reproduced at the device junction.

The impact of injected charge on the junction potential waveform difference between the nonlinear and linear equivalent circuit models was also investigated. An identical formalism was used to quantify the impact of injected charge on the junction potential as per (7). The results of these simulations are plotted in Fig. 6. These results suggest that the difference in junction potential between the nonlinear and linear equivalent circuit models increases as a function of injected charge for the range of values that were investigated.

## IV. DISCUSSION

The intracellular action potential waveform is reproduced at the junction without significant distortion when no action po-

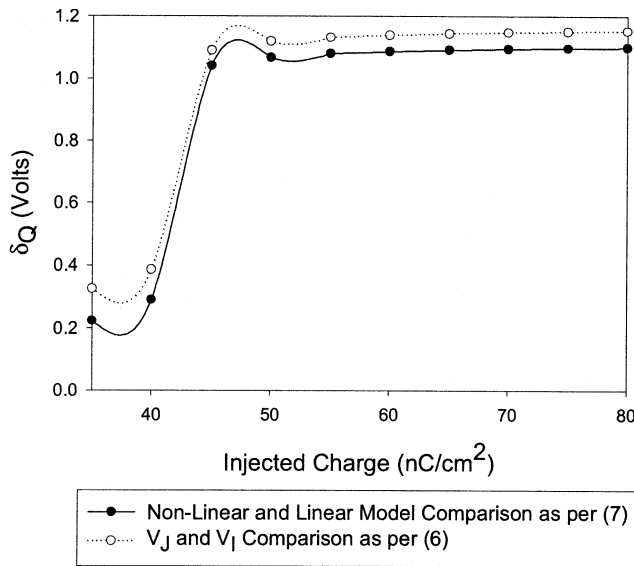


Fig. 6. Norm of the difference between the intracellular potential  $V_I$  and the junction potential  $V_J$ , as well as the norm of the difference in junction potentials  $V_J$  between the nonlinear and linear equivalent circuit models as a function of injected charge. These curves quantify the effectiveness of the linear circuit approximation at reproducing the junction potential  $V_J$  calculated from the nonlinear equivalent circuit model, as well as quantifying the reliability with which the intracellular action potential is reproduced at the junction. A membrane capacitance of  $4 \mu\text{F}/\text{cm}^2$  and an extracellular resistivity of  $25 \text{ k}\Omega/\text{cm}$  were used.

tential like transmembrane potential change is initiated in the region of the membrane interfaced with the device. When this type of transmembrane potential change is initiated in the interfaced region, the resultant junction potential waveform can undergo significant distortion due to the phase difference between the intracellular action potential generated by the free membrane region and the action potential like transmembrane potential change generated as a result of the conductance change in the interfaced region.

As the extracellular resistivity  $\rho_J$  and, consequently, the junction seal resistance  $R_J$  increases, the junction node begins to behave more and more like a broad-band open circuit. This characteristic can most easily be observed by examining the magnitude spectrum of the  $V_J/V_I$  transfer function of the linear equivalent circuit model shown in Fig. 2. The overall result is that a high-fidelity reproduction of the action potential is observed at the junction node for large values of the seal resistance, and no significant conductance change is generated in the interfaced region of the membrane. Manipulation of the seal resistance, from a design perspective, would appear to be a promising technique for improving the fidelity of the detected nerve cell action potential. Variation of the extracellular resistivity  $\rho_J$  was used as a theoretical technique to change the seal resistance  $R_J$  in these simulation studies. In a practical neural prosthetic application, the extracellular resistivity parameter would not likely be accessible to design manipulation. The seal resistance could possibly be increased by way of modifying the structure of the interface region to provide a more electrically insulating barrier to the extracellular environment.

Simulation studies of the effects of membrane capacitance suggest that an increase in the membrane capacitance across the

range of values investigated results in a more reliable reproduction of the nerve cell action potential at the junction. This result, as a trend, is consistent with what would be expected for the initial change in membrane potential as a function of membrane capacitance. A specific region of the membrane is more likely to undergo an action potential like conductance change, as a result of the initial transmembrane potential change, for larger initial displacements of the potential across the membrane that are induced by the injected charge. By taking into account the capacitance associated with the free and the interfaced membrane regions, expressions can be written that approximate the initial change in the potential variables  $V_J$ ,  $V_M$ , and  $V_I$ , as per (8), (9), (10), and (11). These expressions can only be used under the condition that the excitation stimulus pulsewidth, in time, is much smaller than the relevant equivalent circuit time constants, as follows:

$$C_{EQ} = \frac{C_P C_{JG}}{C_P + C_{JG}} \quad (8)$$

$$\Delta V_J = Q_T \frac{C_{EQ}}{C_{JG}(C_{EQ} + C_\Psi)} \quad (9)$$

$$\Delta V_M = Q_T \frac{C_{EQ}}{C_P(C_{EQ} + C_\Psi)} \quad (10)$$

$$\Delta V_I = \frac{Q_T}{C_{EQ} + C_\Psi} \quad (11)$$

Fig. 7 illustrates the initial change in the  $V_J$ ,  $V_M$ , and  $V_I$  variables as a function of the membrane capacitance per unit area and the injected charge per unit area. The curves demonstrate the agreement between the theoretical approximations outlined in (8), (9), (10), and (11) and the simulated data.

The resultant initial change in the transmembrane potential across the interfaced region of the membrane is large enough to induce an action potential like conductance change for small values of the membrane capacitance. A membrane capacitance of  $4 \mu\text{F}/\text{cm}^2$  is required before the transmembrane potential change in the interfaced region of the membrane is suppressed. There is a range of smaller membrane capacitance values for which the initial change in the potential across the interfaced region of the membrane is too small to induce a significant conductance change, but an action potential is observed nevertheless. For these cases, the transmembrane potential change induced in the interfaced region of the membrane results from the potential change associated with the action potential in the free region of the membrane. This effect can most easily be understood based on the relationship between  $V_I$ ,  $V_J$ , and  $V_M$ . For the initial condition where the junction potential  $V_J$  is zero,  $V_M = V_I$ . As the membrane capacitance increases, the higher frequency band of the  $V_M/V_I$  transfer function magnitude spectrum decreases. This characteristic effectively prevents a regenerative action potential like conductance change from developing in the interfaced region of the membrane for the higher range of membrane capacitance values investigated. The membrane capacitance is not accessible to design modification; however, the variability in cell membrane capacitance that can be expected for different excitable cells is sufficient motivation to investigate the impact that these variations have on the detected neural signal.

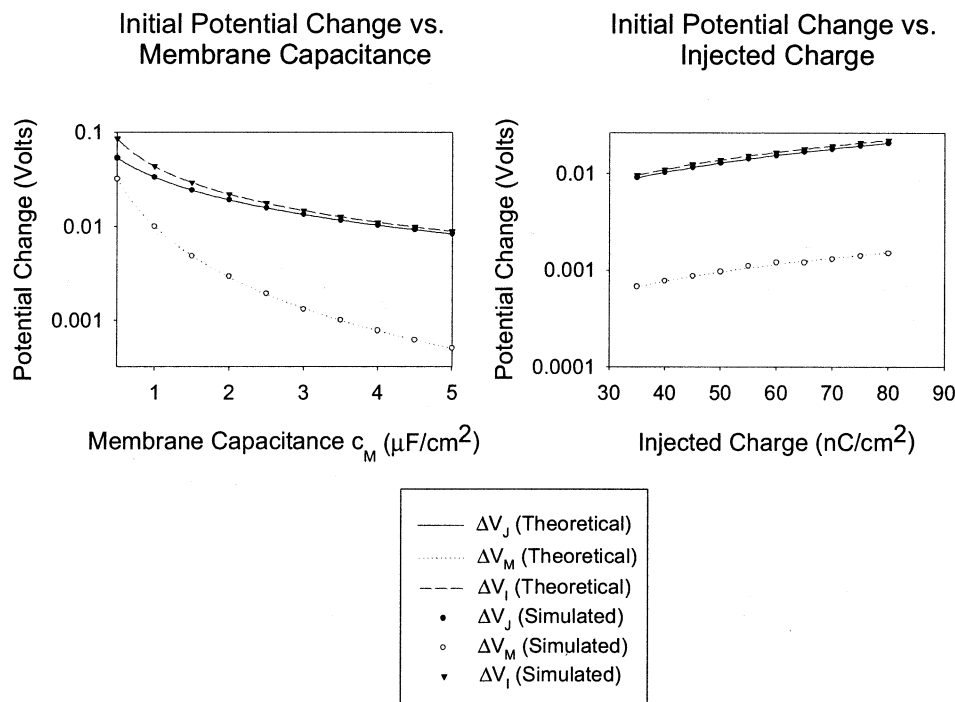


Fig. 7. Initial theoretical and simulated potential change as a function of the membrane capacitance and the injected charge. The graphs illustrate the initial change in potential for the junction potential  $V_J$ , the transmembrane potential  $V_M$ , and the intracellular potential  $V_I$ . For the graph of initial potential change versus membrane capacitance, a stimulus of  $40 \text{ nC}/\text{cm}^2$  was used. The graph of initial potential change versus injected charge was simulated with a membrane capacitance of  $4 \mu\text{F}/\text{cm}^2$ . An extracellular resistivity of  $25 \text{ k}\Omega\text{cm}$  was used for both plots.

Of the parameters that were investigated in this study, the amount of injected charge is the most easily controllable from an experimental perspective. The plot of Fig. 7 suggests that the initial change in the potential across the interfaced region of the membrane would be too small to induce an action potential like transmembrane potential change. Significant conductance changes observed in the interfaced region of the membrane, across the range of values of injected charge that were investigated, were a result of the potential changes in the free region of the membrane that were induced by the free membrane action potential. As the magnitude of the injected charge is increased, there is a consequent increase in the amplitude of the potential change generated in the free membrane region. For larger values of injected charge, this increase in the potential change is sufficient to trigger a significant conductance change in the interfaced region of the membrane. For the simulations where the injected charge was varied, the physical parameters from which the linear equivalent circuit components were calculated were held constant. Consequently, the high-frequency band of the linear equivalent circuit model  $V_M/V_I$  transfer function remained constant. A higher level of injected charge, given the fixed high-frequency band attenuation value, was sufficient to establish an action potential like transmembrane potential change in the interfaced region of the membrane.

Overall, the simulation results are consistent with the hypothesis, based on empirical observations, made by Weis and Fromherz [8]. Under certain conditions, the interfaced region of the membrane behaves in a quasistatic fashion. It is this quasistatic behavior that allows for the applicability of a linear

equivalent circuit modeling approach. The results based on the model and simulation study presented here suggest that a linear circuit modeling approach is not generally applicable under all circumstances.

## REFERENCES

- [1] D. R. McNeal, "Analysis of a model for excitation of myelinated nerve," *IEEE Trans. Biomed. Eng.*, vol. BME-23, pp. 329–336, July 1976.
- [2] W. M. Grill and J. T. Mortimer, "Stimulus waveforms for selective neural stimulation," *IEEE Eng. Med. Biol. Mag.*, vol. 14, pp. 375–385, Aug. 1995.
- [3] E. N. Warman, W. M. Grill, and D. Durand, "Modeling the effects of electric fields on nerve fibers: Determination of excitation thresholds," *IEEE Trans. Biomed. Eng.*, vol. 39, pp. 1244–1254, Dec. 1992.
- [4] J. D. Sweeney, D. A. Ksienski, and J. T. Mortimer, "A nerve cuff technique for selective excitation of peripheral nerve trunk regions," *IEEE Trans. Biomed. Eng.*, vol. 37, pp. 706–715, July 1990.
- [5] R. B. Szlavik and H. de Bruin, "The effect of stimulus current pulse width on nerve fiber size recruitment patterns," *Med. Eng. Phys.*, vol. 21, pp. 507–515, Sept. 1999.
- [6] J. V. Basmajian, *Muscles Alive*. Baltimore, MD: Williams & Wilkins, 1978.
- [7] P. Fromherz and A. Stett, "Silicon-neuron junction: capacitive stimulation of an individual neuron on a silicon chip," *Phys. Rev. Lett.*, vol. 75, no. 8, pp. 1670–1673, 1995.
- [8] R. Weis and P. Fromherz, "Frequency dependent signal transfer in neuron transistors," *Phys. Rev. E*, vol. 55, no. 1, pp. 877–889, Jan. 1997.
- [9] S. Vassanelli and P. Fromherz, "Transistor records of excitable neurons from rat brain," *Appl. Phys. A*, vol. 66, pp. 459–463, 1998.
- [10] P. Fromherz, "Extracellular recording with transistors and the distribution of ionic conductances in a cell membrane," *Eur. Biophys. J.*, vol. 28, pp. 254–258, 1999.
- [11] R. Schatzthauer and P. Fromherz, "Neuron-silicon junction with voltage-gated ionic currents," *Eur. J. Neuroscience*, vol. 10, pp. 1956–1962, 1998.

- [12] A. L. Hodgkin and A. F. Huxley, "Currents carried by sodium and potassium ions through the membrane of the giant axon of loligo," *J. Physiol.*, vol. 116, pp. 449–472, 1952.
- [13] —, "The components of membrane conductance in the giant axon of loligo," *J. Physiol.*, vol. 116, pp. 473–496, 1952.
- [14] —, "The dual effect of membrane potential on sodium conductance in the giant axon of loligo," *J. Physiol.*, vol. 116, pp. 497–506, 1952.
- [15] A. L. Hodgkin, A. F. Huxley, and B. Katz, "Measurement of current-voltage relations in the membrane of the giant axon of loligo," *J. Physiol.*, vol. 116, pp. 424–448, 1952.
- [16] —, "A quantitative description of membrane current and its application to conduction and excitation in nerve," *J. Physiol.*, vol. 117, pp. 500–544, 1952.
- [17] S. Vassanelli and P. Fromherz, "Transistor probes local potassium conductances in the adhesion region of cultured rat hippocampal neurons," *J. Neuroscience*, vol. 19, no. 16, pp. 6767–6773, Aug. 1999.
- [18] T. F. Weiss, *Cellular Biophysics*. Cambridge, MA: MIT Press, 1996.



**Robert B. Szlavik** received the B.Eng. degree (*summa cum laude*) and the M.Eng. and Ph.D. degrees in electrical and computer engineering from McMaster University, Hamilton, ON, Canada, in 1991, 1994, and 1999, respectively.

He is currently Program Chair of Electrical Engineering at Louisiana Tech University, Ruston, LA. He is also affiliated with the Center for Biomedical Engineering and Rehabilitation Science (CyBERS), also at Louisiana Tech University. In addition to his academic duties, he has served as a Scientific Consultant to the Center for Devices and Radiological Health, U.S. Food and Drug Administration. His research interests are in the areas of neural-electronics and the mathematical modeling of the electrical behavior of neurological systems.